Journal of CO_2 Utilization 3–4 (2013) 14–20

Contents lists available at ScienceDirect

Journal of CO_2 Utilization

journal homepage: www.elsevier.com/locate/jcou

Thermokinetic and microstructural analyses of the CO_2 chemisorption on K_2CO_3–Na_2ZrO_3

Pedro Sánchez-Camacho, Issis C. Romero-Ibarra, Heriberto Pfeiffer *

Instituto de Investigaciones en Materiales, Universidad Nacional Autónoma de México, Circuito Exterior s/n, Cd. Universitaria, Del. Coyoacán, CP 04510, México, DF, Mexico

ARTICLE INFO

Article history:
Received 7 March 2013
Received in revised form 9 August 2013
Accepted 11 August 2013
Available online 1 September 2013

Keywords:
CO_2 capture
Microstructure
Sodium zirconate
Thermal analysis
Thermokinetic

ABSTRACT

Sodium zirconate (Na_2ZrO_3) was synthesized via a solid-state reaction. Subsequently, a portion of the prepared Na_2ZrO_3 was mechanically mixed with 5 wt.% potassium carbonate (K_2CO_3). The Na_2ZrO_3 and K-Na_2ZrO_3 samples were characterized, and the CO_2 capture processes were evaluated. The potassium addition did not modify the structural or microstructural characteristics of the Na_2ZrO_3. However, during CO_2 chemisorption, the material presented some important variations that depended on the potassium addition. The maximum CO_2 capture of the Na_2ZrO_3 sample was observed at $T \geq 550$ °C, while the CO_2 capture of the K-Na_2ZrO_3 sample was significantly favored at 400 °C. According to DSC analysis, the CO_2 capture increase observed at lower temperatures was due to the formation of a K–Na carbonate eutectic phase. Additionally, for the samples demonstrating effective CO_2 capture at relatively low temperatures, SEM microstructural analysis demonstrated the formation of a Na_2CO_3–ZrO_2 mesoporous external shell. Moreover, some kinetic parameters were determined. The isothermal data were fitted to a double exponential model related to the direct CO_2 chemisorption (k_1) and diffusion processes (k_2). The K-Na_2ZrO_3 sample presented higher k_1 and k_2 values than Na_2ZrO_3 at all temperatures investigated, confirming that the potassium addition improved the CO_2 capture process. Further, the potassium in Na_2ZrO_3 significantly enhanced the CO_2 capture at approximately 400 °C, in comparison to the Na_2ZrO_3 sample. Finally, it was observed that potassium negatively compromised the chemisorption of CO_2 after several cycles, due to potassium segregation and sublimation.

1. Introduction

In recent decades, the increase in greenhouse gas (GHG) levels in the atmosphere has focused international attention on global warming. Among the various GHGs, CO_2 is the largest contributor with respect to its present content in the atmosphere [1,2].

There are three options for reducing the total CO_2 emitted into the atmosphere, including the use of renewable energy, reductions in CO_2 emissions and enhanced CO_2 sequestration. The first option requires a decrease in the amount of energy consumed, for example, by using energy more efficiently. The second option requires switching to the use of renewable energy sources and non-fossil fuels, such as hydrogen. The third option involves the development of technologies to capture and sequester CO_2 at high concentrations [1,2]. In the case of the third option, several materials have been proposed and analyzed as possible CO_2 captors. The materials proposed include zeolites, activated carbons, hydrotalcites, supported amines and different alkaline and earth alkaline ceramics as promising CO_2 captors due to their favorable sorption behaviors [3–7].

Among the proposed alkaline ceramics, lithium and sodium zirconates (Li_2ZrO_3 [8–13] and Na_2ZrO_3 [14–19]) have attracted the attention of researchers due to their adequate thermal stability and sorption capacity, as well as the ease of fabrication of these materials. This behavior is attributed to their excellent thermal stability, kinetics and CO_2 capture capacity. Specifically, Na_2ZrO_3 exhibits some of the most promising characteristics as a possible CO_2 captor. For example, Na_2ZrO_3 presents better CO_2 capture efficiencies in comparison to lithium-based absorbents [10,14–17,20–22]. Despite the importance of this application, this material has not been deeply analyzed.

However, it has been demonstrated that the CO_2 chemisorption process can be significantly improved in lithium ceramics following the addition of sodium or potassium carbonates [23–26]. The process of CO_2 chemisorption on this mixed alkaline ceramic-carbonate produces a molten carbonate phase, decreasing the partial fusion temperature and increasing the various diffusion processes involved in the CO_2 capture reaction mechanism as a result [17,27]. Therefore, the aim of the present work is to evaluate the CO_2 chemisorption process in the K_2CO_3–Na_2ZrO_3 system at different temperatures. In particular, the microstructural, kinetic and regeneration changes produced in the ceramic are analyzed.

* Corresponding author. Tel.: +52 55 5622 4627; fax: +52 55 5616 1371.
E-mail address: pfeiffer@iim.unam.mx (H. Pfeiffer).

2212-9820/$ – see front matter © 2013 Elsevier Ltd. All rights reserved.
http://dx.doi.org/10.1016/j.jcou.2013.08.003

2. Experimental

Sodium zirconate (Na_2ZrO_3) was prepared via a solid-state reaction. Zirconium oxide (ZrO_2, Aldrich) and sodium carbonate (Na_2CO_3, Aldrich) were mechanically mixed and heat treated at 850 °C for 12 h. For the Na_2CO_3 case, an excess of 10 wt.% was used to compensate the sublimation of sodium during the reaction time [15]. After Na_2ZrO_3 synthesis, part of this sample was mechanically mixed with 5 wt.% potassium carbonate (K_2CO_3, Aldrich). The samples were labeled as follows: the pure sodium zirconate was named Na_2ZrO_3, and the potassium containing sample was labeled K-Na_2ZrO_3.

The Na_2ZrO_3 and K-Na_2ZrO_3 samples were characterized using X-ray diffraction (XRD), scanning electron microscopy (SEM), and nitrogen adsorption. To obtain X-ray diffraction patterns, a diffractometer (Bruker AXS, D8 Advance) coupled to a copper anode X-ray tube was used. The compounds were identified by the corresponding JCPDS files (Joint Committee Powder Diffraction Standards). The microstructural characteristics of Na_2ZrO_3 and K-Na_2ZrO_3 before and after the CO_2 capture process were determined using N_2 adsorption/desorption and SEM. For the N_2 adsorption/desorption experiments, the isotherms were acquired in a Bel-Japan Minisorp II at 77 K using a multipoint technique. The samples were degassed at room temperature for 24 h under vacuum prior to analysis. Then, the SEM images were taken on a JEOL JMS-7600F microscope.

Different CO_2 chemisorption experiments (dynamic and isothermal) were performed using a Q500HR instrument from TA Instruments. Initially, the sodium zirconate samples were dynamically heated from room temperature to 850 °C under a CO_2 atmosphere at 5 °C/min. Then, isothermal experiments were performed to evaluate the effect of potassium on the Na_2ZrO_3-CO_2 reaction mechanism. For isothermal analysis, the samples were initially heated to 850 °C at 50 °C/min with a subsequent isothermal treatment of 15 min under N_2 flow. This procedure was conducted to ensure that all of the samples received an equivalent sintering process prior to performing the CO_2 chemisorption isotherms. Additionally, this heating process desorbed all of the water and CO_2 previously trapped in the samples as a result of the handling processes. After this heating process, each sample was cooled to the respective isothermal temperature to perform an independent CO_2 chemisorption process. Once the sample reached the corresponding temperature, the gas flow was switched from N_2 to CO_2, and the isothermal experiments were performed using a gas flow rate of 60 mL/min. Some of the Na_2ZrO_3-CO_2 isothermal products were re-characterized microstructurally using SEM. Finally, Na_2ZrO_3 and K-Na_2ZrO_3 samples, as well as some of the Na_2ZrO_3-CO_2 and K-Na_2ZrO_3-CO_2 isothermal products, were characterized by thermogravimetric (TGA and DTG) and differential scanning calorimetry (DSC). These experiments were carried out using a previously described thermogravimetric set-up (using N_2 as carrier gas) with DSC equipment from Instrument Specialists Inc. For the DSC experiments, the samples were heated from room temperature to 600 °C at 20 °C/min under an inert argon atmosphere. Finally, different multicycle CO_2 chemisorption–desorption experiments were performed at 400 and 700 °C (chemisorption) and 850 °C (desorption) to elucidate the thermal stability and cyclic performance of both samples.

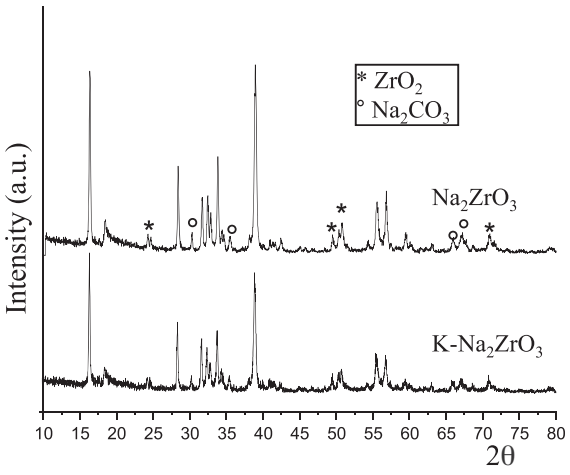

Fig. 1. XRD patterns of the Na_2ZrO_3 and K-Na_2ZrO_3 samples prepared via a solid-state reaction. The secondary phases were labeled with different symbols.

3. Results and discussion

To establish the structural and microstructural characteristics of both sodium zirconates (Na_2ZrO_3 and K-Na_2ZrO_3), the samples were analyzed by XRD, SEM and N_2 adsorption. Fig. 1 shows the XRD patterns of the Na_2ZrO_3 and K-Na_2ZrO_3 samples after thermal treatment at 850 °C and the corresponding potassium addition. The diffraction patterns fitted to JCPDS file 35-0770 corresponds to monoclinic Na_2ZrO_3, although the presence of ZrO_2 and Na_2CO_3 was also observed. The presence of these secondary phases can be attributed to the CO_2 chemisorption process, producing these phases during sample handling, or to an incomplete solid-state reaction process. Additionally, the K-Na_2ZrO_3 diffraction pattern showed was very similar to that of Na_2ZrO_3, as the K_2CO_3 concentration was insufficient for quantification by this technique.

The morphologies and particle sizes of the samples were analyzed by SEM (Fig. 2). Na_2ZrO_3 and K-Na_2ZrO_3 presented similar morphologies and particle sizes. The particles presented dense

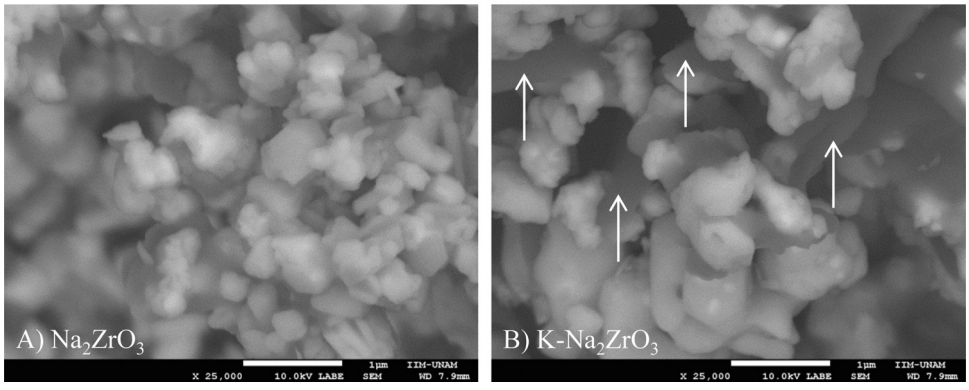

Fig. 2. Backscattered electron images of the Na_2ZrO_3 (A) and K-Na_2ZrO_3 (B) samples. The arrows indicates the presence of flat dark particles associated to the K_2CO_3.

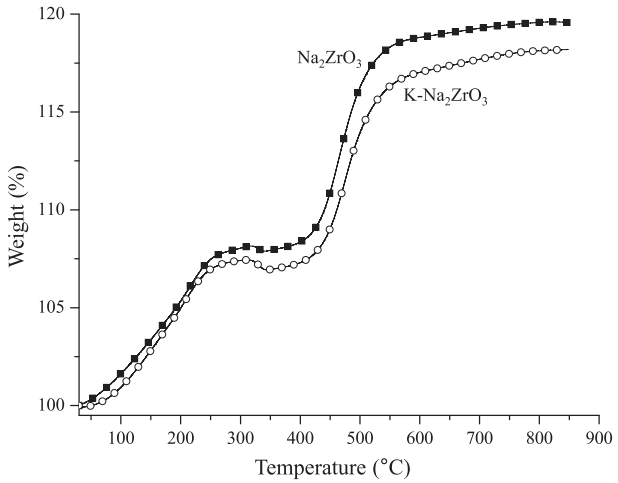

Fig. 3. Dynamic thermogravimetric curves of Na_2ZrO_3 and K-Na_2ZrO_3 samples, between 30 and 850 °C into a CO_2 flux.

polyhedral morphologies with an average particle size of approximately 500–800 nm. These particles produced agglomerates measuring approximately 5 μm. In the K-Na_2ZrO_3 sample, some flat dark particles were observed, which were associated with the presence of K_2CO_3. The surface morphology was analyzed via N_2 adsorption. The Na_2ZrO_3 and K-Na_2ZrO_3 samples presented surface areas of 1.5 and 1.1 m^2/g, respectively, according to the BET model [28,29].

After characterizing the structures and microstructures of Na_2ZrO_3 and K-Na_2ZrO_3, both materials were thermally analyzed under CO_2 flow (Fig. 3). Na_2ZrO_3 and K-Na_2ZrO_3 presented typical and similar CO_2 dynamic chemisorption behaviors. The thermograms show two different weight increases. The first weight increase was produced between 30 and 290 °C, while the second was produced at temperatures higher than 400 °C. The first process was associated with the chemisorption of CO_2 on the particle surface. At this point, a thin Na_2CO_3 external shell, mixed with ZrO_2, is likely produced over the Na_2ZrO_3 particle surface. In contrast, the second weight increase was produced at $T > 400$ °C, as a result of the activation of diffusion processes [27]. Although the potassium addition did not appear to significantly modify the dynamic CO_2 chemisorption, nonetheless, between 290 and 400 °C, an interesting difference in the thermograms can be observed. While the Na_2ZrO_3 sample lost 0.29 wt.% in this temperature range, the K-Na_2ZrO_3 sample lost 0.82 wt.%, which is approximately three times the weight loss. This result may be associated with a partial CO_2 desorption process produced over the particle surface, which indicates a different CO_2 absorption–desorption equilibrium than that observed for the Na_2ZrO_3 sample. A similar effect was previously observed in the Na_2ZrO_3 and $Na_2(Zr\text{-}Al)O_3$ systems [30].

To analyze the influence of the potassium addition on the CO_2 capture process in Na_2ZrO_3, different isothermal experiments were performed between 300 and 700 °C (Fig. 4). For the Na_2ZrO_3 case (Fig. 4A), all of the isothermal experiments followed a typical exponential behavior, where the CO_2 chemisorption increased as a function of temperature. At 300 and 400 °C, the isotherms did not reach equilibrium after 3 h, and the weight increments were 2.0 and 14.3 wt.%, respectively. Later, a more rapidly increasing exponential behavior was obtained for the sample treated at 500 °C, which significantly increased the CO_2 chemisorption behavior (18.5 wt.%). Treating the sample isothermally at 600 °C resulted in a partial decrease in the CO_2 chemisorption. This atypical phenomenon has recently been associated with a Na_2CO_3–ZrO_2 external shell densification process, as the external shell presents a degree of mesoporosity at $T \leq 550$ °C, which allows for

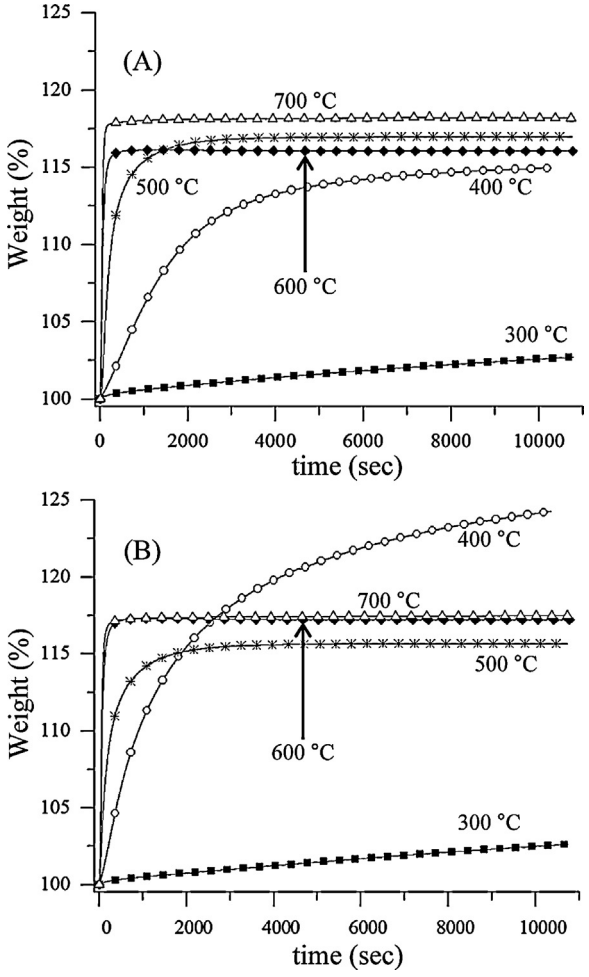

Fig. 4. Isothermal analyses at different temperatures (300–700 °C) of the Na_2ZrO_3 (A) and K-Na_2ZrO_3 (B) samples.

higher CO_2 chemisorption [17,31]. Finally, at 700 °C, the intercrystalline diffusion processes are activated, recovering the CO_2 chemisorption behavior, which increases as a function of temperature.

However, although the K-Na_2ZrO_3 sample (Fig. 4B) presented a similar exponential behavior, some significant variations were also observed. At 300 °C, the amount of CO_2 chemisorbed was very poor (2.6 wt.%), as in the Na_2ZrO_3 case. Nevertheless, the K-Na_2ZrO_3 sample presented the highest CO_2 chemisorption at 400 °C, with a value of 24.2 wt.%. Later, between 500 and 700 °C, the CO_2 chemisorption values decreased, although the CO_2 chemisorption process occurred faster during the initial minutes of the test than the behavior observed at 400 °C. It has been reported that the process of CO_2 absorption in Na- or K-containing lithium ceramics produces a molten lithium–sodium or lithium–potassium carbonate phase [23–26,31]. The K and Na additions usually do not exceed 5–10 wt.% because the main intention of adding these elements is to improve the diffusion processes due to partial melt processes. Therefore, to demonstrate that the partial melting process of the Na_2CO_3–K_2CO_3 eutectic phase is present in the Na_2ZrO_3 external shell, different DSC experiments were carried out. Additionally, the potassium addition produced more rapid densification of the porosity in the Na_2CO_3–ZrO_2 external shell because the isothermal capture of CO_2 in the K-Na_2ZrO_3 sample decreased at 500 °C and not at 600 °C, as in the Na_2ZrO_3 case.

Fig. 5 shows different DSC analyses of the Na_2ZrO_3 and K-Na_2ZrO_3 samples. In the K-Na_2ZrO_3 case, the sample was analyzed

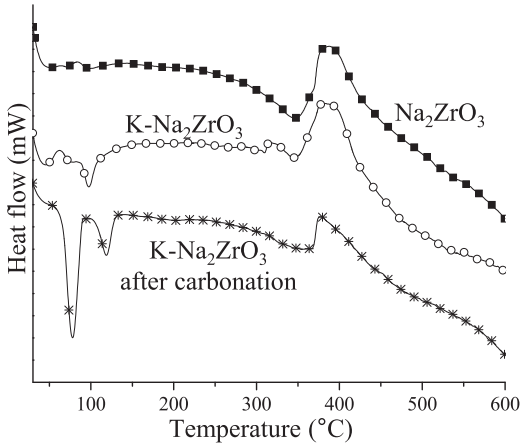

Fig. 5. DSC analysis of the Na_2ZrO_3 and K-Na_2ZrO_3 samples and the K-Na_2ZrO_3 sample previously treated at 400 °C into a CO_2 flux.

before and after the CO_2 capture processes. Initially ($T < 150$ °C), the three samples presented calorimetric behaviors that fit very well with the thermogravimetric experiments. The different peaks observed in this temperature range correspond to superficial or crystalline dehydration processes. After the carbonation process, the K-Na_2ZrO_3 sample presented the highest endothermic dehydration peaks, which are associated with the water affinity presented by the Na_2CO_3 produced over the highly hygroscopic Na_2ZrO_3 particle surface. However, additional information that can be obtained from the decarbonation peaks is observed below 300 °C. The Na_2ZrO_3 sample presented a single well-defined endothermic peak with an onset temperature of 255 °C and an enthalpy (ΔH) value of 179.3 kJ/mol. However, the K-Na_2ZrO_3 sample presented a double peak, which corresponds with the superficial Na_2CO_3 presence because the Na_2ZrO_3 sample had added K_2CO_3. These two peaks could not be separated for parameter determination, so the onset temperature and ΔH values obtained were 247 °C and 125.2 kJ/mol. It is clear that both the onset temperature and ΔH were reduced by the K_2CO_3 addition, which is in agreement with the formation of the carbonate solid solution [33]. In the third case (K-Na_2ZrO_3 sample isothermally treated at 400 °C in a CO_2 atmosphere), the corresponding ΔH value was 100.5 kJ/mol. Thus, the ΔH value continued to decrease, as the Na_2CO_3–K_2CO_3 eutectic phase was completely formed during previous carbonations.

To complete the analysis of sample characterization, Figs. 6 and 7 present SEM images of the Na_2ZrO_3 and K-Na_2ZrO_3 samples following isothermal treatment at 500 °C in a CO_2 atmosphere. The backscattered electron image (BSEI) confirms the presence of two phases in the surface region, due to the different contrasts observed in the particles. These two phases are identified as ZrO_2 and Na_2CO_3 or K-containing Na_2CO_3 (the eutectic carbonate phase), as they are the Na_2ZrO_3 carbonation products. In this case, the Na_2ZrO_3 phase is not identifiable in the image because the remaining Na_2ZrO_3 must be located within the particle's core, as it has been reported in other micrometric CO_2-alkaline ceramic reaction models [4,27]. The difference in observed contrast arises from the difference in the mean atomic number, $\bar{Z}$, of ZrO_2 ($\bar{Z} = 18.666$) relative to the mixed carbonate phase (for the Na_2CO_3 $\bar{Z} = 8.666$, which is the majority phase). The $\bar{Z}$ difference produces changes in the backscattered electron coefficient, η, of the two phases [33,34]. Thus, the dark phase corresponds to the mixed carbonate phase, while the lighter phase is ZrO_2. Although the K-Na_2ZrO_3 particle size did not change significantly after the

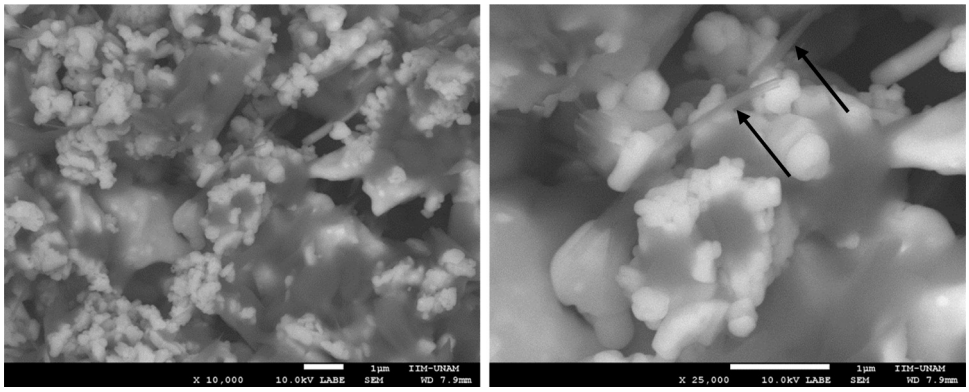

Fig. 6. Backscattered electron images of the Na_2ZrO_3 sample isothermally treated at 500 °C into a CO_2 atmosphere. The arrows indicate the filament-like particle formations.

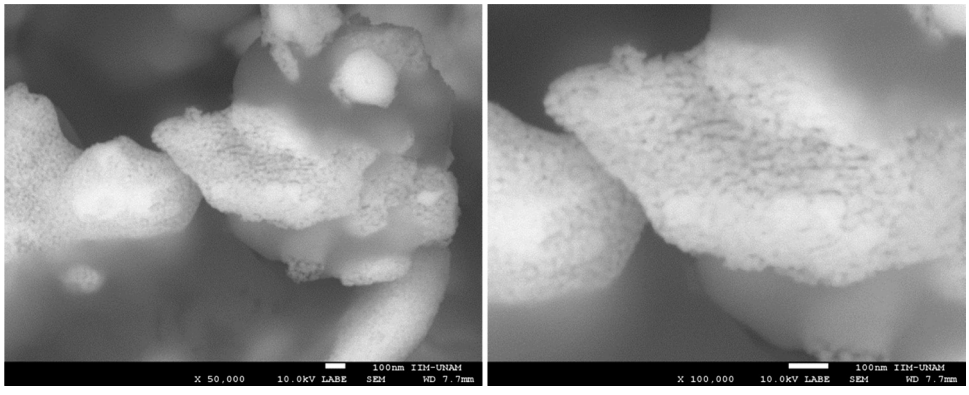

Fig. 7. Backscattered electron images of the K-Na_2ZrO_3 sample isothermally treated at 500 °C into a CO_2 atmosphere.

Table 1
Kinetic parameters obtained from the isothermal fitting to the double exponential model.

T (°C)	k_1 (s^{-1})	k_2 (s^{-1})	R^2
Na_2ZrO_3			
300	0.00045	0.00012	0.99876
400	0.00043	0.00026	0.99908
500	0.00271	0.00056	0.99688
600	0.00953	0.00184	0.99153
700	0.01496	0.0001	0.94342
K-Na_2ZrO_3			
300	0.00832	0.00005	0.9997
400	0.00113	0.00021	0.99992
500	0.00659	0.00127	0.9998
600	0.01495	0.00132	0.99233
700	0.01904	0.00025	0.98244

carbonation process, the mixed carbonate phase (dark phase) produced layered-like and filamentous structures, and the presence of mesoporosity was evidenced (see Fig. 7). These results are in good agreement with a previous report in which the presence of an external mesoporous phase was reported in Na_2ZrO_3 as a result of carbonation at $T \leq 550$ °C [17].

To analyze whether the potassium addition affects the CO_2 capture process of Na_2ZrO_3, the isothermal data were fitted to a double exponential model, as a result of the two different processes taking place: (1) CO_2 chemisorption occurs over the Na_2ZrO_3 particle surface (k_1), which induces the formation of an external shell of alkaline carbonate and ZrO_2, and (2) the CO_2 chemisorption is kinetically controlled by diffusion processes (k_2) [35–39]:

$$y = A\ \exp^{k_1 t} + B\ \exp^{k_2 t} + C$$

where y represents the weight percentage of chemisorbed CO_2, t is the time, and k_1 and k_2 are the exponential constants for the CO_2 chemisorption over the Na_2ZrO_3 particle surface and the chemisorption of CO_2 kinetically controlled by diffusion processes, respectively. Additionally, the pre-exponential factors A and B indicate the intervals over which each process controls the whole CO_2 capture process, and the constant C denotes the y-intercept. All of the exponential constant parameters are presented in Table 1. It can be observed that, independently of the potassium addition, the direct CO_2 chemisorption constant values (k_1) are higher than that

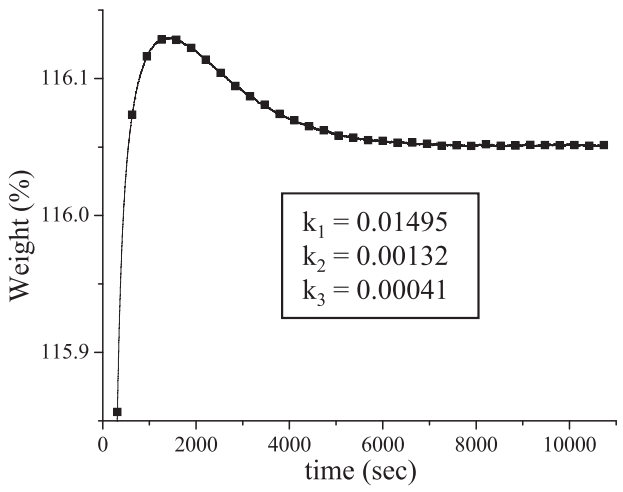

Fig. 8. Isotherm of the K-Na_2ZrO_3 sample treated at 600 °C into a CO_2 flux. The sample was fitted to a triple exponential model, as it was evidenced in the presence of an additional process; the CO_2 desorption.

of the CO_2 chemisorption kinetically controlled by diffusion processes (k_2). This result is in good agreement with previous reports [35,36,39] and indicates that the rate limiting step is the CO_2 chemisorption, which is kinetically controlled by diffusion processes. However, at 400 °C, the k_1 values decreased independently of the potassium addition. This effect is attributed to the partial superficial desorption of CO_2 observed during dynamic thermogram analysis in the same temperature range. Additionally, it should be noted that the k_1 and k_2 constants were different for the Na_2ZrO_3 and K-Na_2ZrO_3 samples. K-Na_2ZrO_3 presented higher k_1 and k_2 values than Na_2ZrO_3 throughout the entire temperature range, confirming that potassium addition improves the CO_2 capture process. It should be noted that the potassium addition enhances the initial reaction process upon melting because the liquid phase promotes the superficial CO_2 reaction and the porous diffusion processes.

Once the high-temperature isotherms were analyzed more thoroughly, a third process was identified, i.e., CO_2 desorption. This process was evidenced by a slight decrease in the weight ($T \geq 600$ °C, see Fig. 8). The chemisorption/desorption equilibrium was not present at lower temperatures because there may not have been a desorption process. Therefore, this isotherm showed three different trends. At short times, the increase in weight was equal to that observed for the other isotherms, after fitting these data to a double exponential model. The k_1 and k_2 values obtained fitted the previous analysis very well. Then, the curve showed a lag period, in which the absorption did not increase. At long times, the desorption process became evident, although it was minimal. The samples only lost between 0.03 and 0.05 wt.%, due to the considerably low value of k_3 (0.00041 s^{-1}). Thus, using the entire data range, a different fitting was performed with a triple exponential model. This model considers three processes, including (1) the CO_2 chemisorption over the sample particle surface, (2) the CO_2 chemisorption that is kinetically controlled by diffusion processes and (3) the CO_2 desorption.

Finally, multicyclic experiments were performed with the K-Na_2ZrO_3 sample. The CO_2 chemisorption process was performed at 400 and 700 °C, but it was necessary to perform the desorption process at 850 °C because at lower temperatures, the desorption of CO_2 was not produced. Fig. 9A shows the cyclic performance of the K-Na_2ZrO_3 sample. It can be observed that the CO_2 capture efficiency decreased significantly after each chemisorption–desorption cycle at 400 °C. This effect is associated with the potassium and sodium segregations and the sublimation of potassium that occurred during the desorption processes performed at 850 °C. Previous multicyclic reports on alkaline ceramics, specifically, lithium ceramics such as K-Li_4SiO_4 and K-Li_2ZrO_3, have demonstrated better cycling stabilities [4,10,18,24,32,36,40–44]. However, in such cases, the desorption temperatures were always equal to the chemisorption temperatures ($T \leq 630$ °C). At this temperature, the influence of the potassium–lithium segregation and sublimation processes must be reduced. Nevertheless, it is not possible to use the same conditions for Na_2ZrO_3-CO_2 because the Na_2CO_3 decomposition temperature is approximately 850 °C.

When Na_2ZrO_3 and K-Na_2ZrO_3 were tested at 700 °C, the cycling stability appeared to be sufficient (Fig. 9B). However, the CO_2 capture decreased in both cases as a function of the cycle number; the CO_2 desorption capacity of the K-Na_2ZrO_3 sample decreased, while the Na_2ZrO_3 sample appeared to partially decompose. The CO_2 capture of Na_2ZrO_3 decreased from 4.76 to 4.2 mmol/g, while that of K-Na_2ZrO_3 decreased from 4.48 to 4.01 mmol/g (Fig. 9C). This effect may be associated with different effects, such as the particle sintering process and the Na and K sublimation processes. Hence, the potassium addition does not seem to produce any significant change, as the CO_2 capture behavior is mainly produced

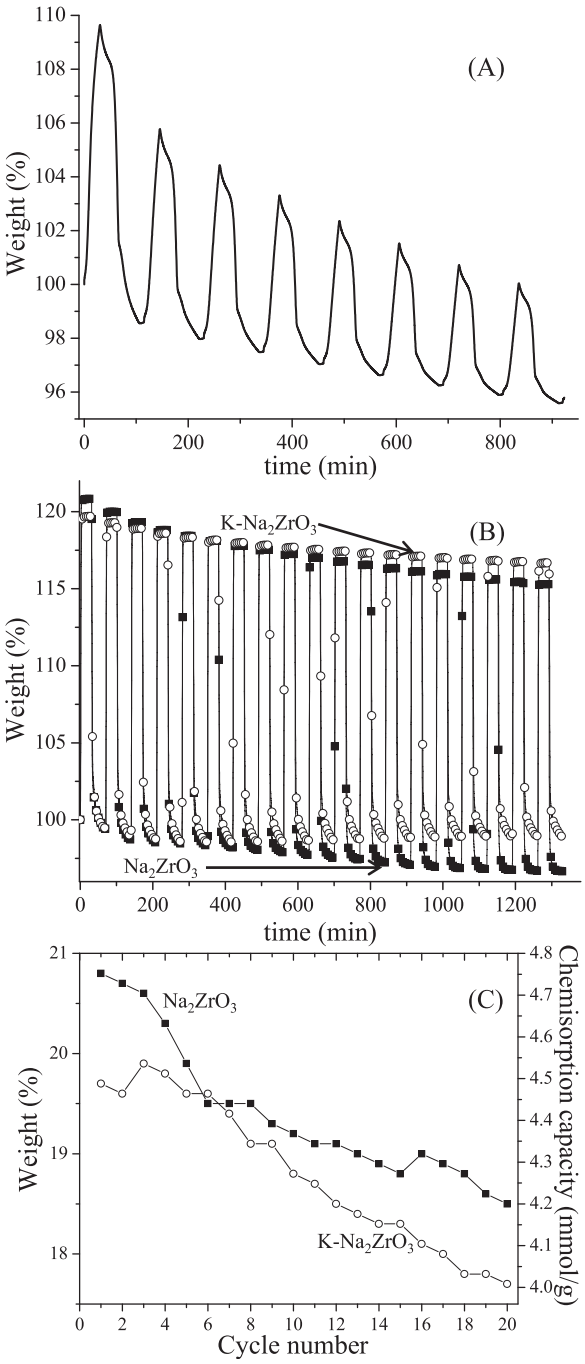

Fig. 9. Multicycle performance of CO_2 chemisorption/desorption in K-Na_2ZrO_3, in which the consecutive CO_2 chemisorptions were performed at 400 °C for 30 min, while the desorption processes were performed at 850 °C over 30 min into a N_2 flux (A and B). Na_2ZrO_3 and K-Na_2ZrO_3 multicycles experiments, in which the CO_2 chemisorption were performed at 700 °C (C).

by intercrystalline diffusion processes at this temperature range [17].

4. Conclusions

Na_2ZrO_3 was synthesized via a solid-state reaction. Further, part of the Na_2ZrO_3 sample was also mechanically mixed with K_2CO_3 (5 wt.%). Then, both samples were characterized structurally and microstructurally, and the CO_2 capture process was evaluated. Although the CO_2 dynamic experiments did not show significant differences following the addition of potassium, the isothermal analysis did. The K-Na_2ZrO_3 sample treated at 400 °C captured more CO_2 than the Na_2ZrO_3 original sample over all of the analyzed temperature range. Na_2ZrO_3 usually presents the best CO_2 capture behavior at $T \geq 550$ °C. Under these conditions, the CO_2 capture of the samples in this work was very close to 100% efficiency (specifically, 98%). Independent of the potassium addition, the direct CO_2 chemisorption constant values (k_1) were found to be higher than that of the CO_2 chemisorption that was kinetically controlled by diffusion processes (k_2). The increased CO_2 chemisorption was attributed to the formation of a K–Na carbonate eutectic phase, which can produce a partial liquid phase, favoring the diffusion of CO_2 through the mesoporous external shell. This possibility was supported by various DSC and isothermal analyses and SEM observations.

Conversely, the potassium addition produced a CO_2 desorption process at T 600 °C, which was not observed in the Na_2ZrO_3 sample. Finally, multicycle experiments were performed at 400 and 700 °C to elucidate the thermal stability and CO_2 capture efficiency through different cycles in both ceramics. In this case, it was observed that the addition of potassium did not stabilize the CO_2 chemisorption behavior after several cycles, due to potassium segregation, and sublimation developed during CO_2 desorption at 850 °C. Therefore, the addition of K to Na_2ZrO_3 significantly enhances the CO_2 capture behavior of the material at approximately 400 °C, relative to that of the Na_2ZrO_3 sample, although the thermal and cyclic stability of this sample were compromised.

Acknowledgements

This work was financially supported by the project PAPIIT-UNAM number IN-102313. Authors thank to A. Tejeda and O. Novelo for technical help.

References

[1] H. Yang, Z. Xu, M. Fan, R. Gupta, R.B. Slimane, A.E. Bland, I. Wright, J. Environ. Sci. 20 (2008) 14–27.
[2] A. Yamasaki, J. Chem. Eng. Jpn. 36 (2003) 361–375.
[3] D.M. D'Alessandro, B. Smit, J.R. Long, Angew. Chem. Int. Ed. 49 (2010) 2–27.
[4] B.N. Nair, R.P. Burwood, V.J. Goh, K. Nakagawa, T. Yamaguchi, Prog. Mater. Sci. 54 (2009) 511–541.
[5] S. Choi, J.H. Drese, C.W. Jones, ChemSusChem 2 (2009) 796–854.
[6] Q. Wang, J. Luo, Z. Zhong, A. Borgna, Energy Environ. Sci. 4 (2011) 42–55.
[7] N. Hedin, L.J. Chen, A. Laaksonen, Nanoscale 2 (2010) 1819–1841.
[8] M. Olivares-Marín, M. Castro-Díaz, T.C. Drage, M.M. Maroto-Valer, Sep. Purif. Technol. 73 (2010) 415–420.
[9] Q. Xiao, Y. Liu, Y. Zhong, W. Zhu, J. Mater. Chem. 21 (2011) 3838–3842.
[10] H.R. Radfarnia, M.C. Iliuta, Ind. Eng. Chem. Res. 50 (2011) 9295–9305.
[11] A. Iwan, H. Stephenson, W.C. Ketchie, A.A. Lapkin, Chem. Eng. J. 146 (2009) 249–258.
[12] S. Wang, C. An, Q.H. Zhang, J. Mater. Chem. A 1 (2013) 3540–3550.
[13] L. Guo, X. Wang, S. Zhang, C. Zhong, L. Li, J. Mater. Sci. 46 (2011) 6960–6963.
[14] T. Zhao, E. Ochoa-Fernández, M. Rønning, D. Chen, Chem. Mater. 19 (2007) 3294–3301.
[15] I. Alcérreca-Corte, E. Fregoso-Israel, H. Pfeiffer, J. Phys. Chem. C 112 (2008) 6520–6525.
[16] G.G. Santillán-Reyes, H. Pfeiffer, Int. J. Greenhouse Gas Control 5 (2011) 1624–1629.
[17] L. Martínez-dlCruz, H. Pfeiffer, J. Phys. Chem. C 116 (2012) 9675–9680.
[18] E. Ochoa-Fernández, M. Rønning, X. Yu, T. Grande, D. Chen, Ind. Eng. Chem. Res. 47 (2008) 434–442.
[19] E. Ochoa-Fernandez, H.K. Rusten, H.A. Jakobsen, M. Ronning, A. Holmen, D. Chen, Catal. Today 106 (2005) 41–46.
[20] M. Khokhani, R.B. Khomane, B.D. Kulkarni, J. Sol-Gel Sci. Technol. 61 (2012) 316–320.
[21] E.P. Lokshin, V.N. Lebedev, Russ. J. Appl. Chem. 85 (2012) 1003–1010.
[22] H.R. Radfarnia, M.C. Iliuta, Sep. Purif. Technol. 93 (2012) 98–106.
[23] K. Nakagawa, T. Ohashi, Electrochemistry 67 (1999) 618–621.
[24] G. Pannocchia, M. Puccini, M. Seggiani, S. Vitolo, Ind. Eng. Chem. Res. 46 (2007) 6696–6701.
[25] J. Ida, R. Xiong, Y.S. Lin, Sep. Purif. Technol. 36 (2004) 41–51.
[26] V.L. Mejía-Trejo, E. Fregoso-Israel, H. Pfeiffer, Chem. Mater. 20 (2008) 7171–7176.
[27] J. Ortiz-Landeros, T. Ávalos-Rendón, C. Gómez-Yáñez, H. Pfeiffer, J. Therm. Anal. Calorim. 108 (2012) 647–655.

[28] S. Lowell, J.E. Shields, M.A. Thomas, Characterization of Porous Solids and Powders: Surface Area, Pore Size and Density; Particle Technology Series, Kluwer Academic Publishers, London, 2004.
[29] E.M. McCash, Surface Chemistry, Oxford University Press, Oxford, UK, 2002.
[30] B. Alcántar-Vázquez, C. Diaz, I.C. Romero-Ibarra, E. Lima, H. Pfeiffer, J. Phys. Chem. C (2013), http://dx.doi.org/10.1021/jp4053924.
[31] F. Durán-Muñoz, I.C. Romero-Ibarra, H. Pfeiffer, J. Mater. Chem. A 1 (2013) 3919–3925.
[32] M. Olivares-Marín, T.C. Drage, M.M. Maroto-Valer, Int. J. Greenhouse Gas Control 4 (2010) 623–629.
[33] W. Eitel, W. Skaliks, Z. Anorg. U. Allgem. Chem. 183 (1929) 270–272.
[34] J.I. Goldstein, D.E. Newbury, P. Echlin, D.C. Joy, C. Fiori, E. Lifshin, Scanning Electron Microscopy and X-ray Microanalysis, Plenum, New York, 1981.
[35] T.L. Ávalos-Rendon, J. Casa-Madrid, H. Pfeiffer, J. Phys. Chem. A 113 (2009) 6919–6923.
[36] X.S. Yin, Q.H. Zhang, J.G. Yu, Inorg. Chem. 50 (2011) 2844–2850.
[37] Z. Qi, H. Daying, L. Yang, Y. Qian, Z. Zibin, AIChE J. 59 (2013) 901–911.
[38] D.K. Lee, I.H. Baek, W.L. Yoon, Chem. Eng. Sci. 59 (2004) 931–942.
[39] R. Rodriguez-Mosqueda, H. Pfeiffer, J. Phys. Chem. A 114 (2010) 4535–4541.
[40] T. Ávalos-Rendón, V.H. Lara, H. Pfeiffer, Ind. Eng. Chem. Res. 51 (2012) 2622–2630.
[41] S.Z. Kang, T. Wu, X. Li, J. Mu, Mater. Lett. 64 (2010) 1404–1409.
[42] M. Kato, K. Nakagawa, K. Essaki, Y. Maezawa, S. Takeda, R. Kogo, Y. Hagiwara, Int. J. Appl. Ceram. Technol. 2 (2005) 467–473.
[43] X.S. Yin, S.P. Li, Q.H. Zhang, J.G. Yu, J. Am. Ceram. Soc. 93 (2010) 2837–2842.
[44] X.S. Yin, S.P. Li, Q.H. Zhang, J.G. Yu, Ind. Eng. Chem. Res. 49 (2010) 6593–6598.